Proceedings of 20th International Congress on Acoustics, ICA 2010

23-27 August 2010, Sydney, Australia

A mesh-less self-adaptive boundary element quadrature scheme for underwater noise prediction

Yingsan Wei[1]*, Yongsheng Wang[1]

(1) Department of Mechanical Engineering, Naval University of Engineering, Wuhan 430033, P R China

PACS: 43.30 Jx, 43.40.Ey, 43.40.Rj, 43.40.Tm.

ABSTRACT

When general boundary element method(BEM) is applied to Helmholtz integral equation(HIE), integration singularity and hyper-singularity occurs. A self-adaptive Gauss quadrature algorithm was proposed to overcome the singularity. In this technique, the initial singular boundary element (*father element*) was divided into temporary refined small elements(*children elements*), and the integral on initial element was transformed to Gauss quadrature on *children elements*. The *children elements* can further be divided into smaller elements until integral solution converged at an allowable tolerance without increase boundary elements number as the refined *children elements* were cleared simultaneously when singular integration finished. Taking the advantages of this technique, the radiation surface can be coarsely meshed so as to reduce elements number and computational effort. Then the convergence behavior and application scope of this adaptive scheme was researched, and it is showed that this adaptive scheme can only be applied to singular or weak-singular integration. A numerical case about the sound radiation of a uniformly pulsating sphere was investigated to validate the adaptive algorithm, and numerical solutions agree well with analytical solutions with relative error less than 1.5dB. Then BEM coupled with FEM were applied to predict submarine vibration-noise considering fluid-structure interaction effects. By visualization the near-field sound pressure distribution, high sound pressure area was localized. Finally, the underwater radiated sound power was calculated and the peak frequencies were identified. Reduction of the engine periodic-isolator's stiffness can effectively transfer the sound power of peak frequencies to band-spectrum and the vibration noise of the line spectrum is controlled.

INTRODUCTION

Since the early sixties BEM has been used in wave propagation and scattering problem by Jaswon, Symm [1,2]. Chen and Chertock [3,4] firstly use BEM to solve acoustic radiation and scattering problem. Since BEM requires only modeling the boundary surface of radiation object rather than the entire field domain, so BEM is widely used to solve the HIE for predicting noise. However, when BEM is applied to calculate near-field sound pressure, singularity and hyper-singularity of HIE occurs [5-9]. Recently Visser [10] proposed a local adaptive Gauss quadrature to overcome singular and hyper-singular integration. In this paper a global self-adaptive BEM quadrature algorithm is introduced to overcome solution singularity, then the convergence behavior and application scope of the algorithm is researched. Results show that adaptive Gauss quadrature can be applied to singular or weak singular integration, and for hyper-singular integration, non convergent solution is inevitable.

SELF-ADAPTIVE GAUSS QUADRATURE FOR HELMHOLTZ SINGULAR INTEGRATION

Boundary Element Formulation

In a homogeneous medium at rest and considering the three-dimensional linear time-harmonic problem of acoustics, the governing differential equation is the Helmholtz equation:

$$\Delta u(\vec{x}) + k^2 u(\vec{x}) = 0\,, \quad \vec{x} \in D \subset \mathbb{R}^3 \tag{1}$$

where $u(\vec{x})$ represents the complex acoustic pressure(often called pressure for short), Δ is Laplace operator, $k = \omega / c$ denotes the wave number, ω is the angular frequency, c is the speed of sound in fluid, and D stands for the three-dimensional domain of propagation, ∂D denotes the boundary of D .Herein Neumann problem in external acoustic is considered, so the boundary condition is satisfied:

$$\partial u(\vec{x}) / \partial n(\vec{x}) = sk v_n(\vec{x})\,, \qquad \vec{x} \in \partial D \tag{2}$$

where $n(\vec{x})$ denotes the unit normal at $\vec{x} \in \partial D$ and directed into D , $v_n(\vec{x})$ is the normal velocity at $\vec{x}$, $s = i\rho_f c$ where ρ_f is the density of the medium of propagation. In the case when the domain D is unbounded , the above problem has to satisfied the *Sommerfeld radiation condition* as $r_f \to \infty$ for 3-D problems, that:

$$u(\vec{x}) = O(r_f^{-1})\,, \partial u(\vec{x}) / \partial r_f - iku(\vec{x}) = o(r_f^{-1}) \tag{3}$$

Then Helmholtz equation can be solved:

$$\alpha(\bar{x})u(\bar{x}) = \int_S [G(r)\frac{\partial u(\bar{y})}{\partial n(\bar{y})} - \frac{\partial G(r)}{\partial n(\bar{y})}u(\bar{y})]\, dS \tag{4}$$

where $\bar{y}$ is so called *source points* located on the boundary surface and $\bar{x}$ is *field points* in the fluid domain, $\alpha(\bar{x})$ is a geometry related coefficient, $\alpha(\bar{x})$ =1 when $\bar{x} \in \mathrm{D}$, $\bar{x} \notin \partial\mathrm{D}$, $\alpha(\bar{x}) = 1/2$ when $\bar{x} \in \partial\mathrm{D}$, and $\alpha(\bar{x}) = 0$ when $\bar{x} \notin \mathrm{D} \bigcup \partial\mathrm{D}$. $G(r)$ is the Green function in free space, that:

$$G(\bar{y},\bar{x}) = -e^{ikr}/4\pi r \tag{5}$$

$r = \left\|\bar{x} - \bar{y}\right\|$ is the 2-norm of vector $\bar{r} = \bar{x} - \bar{y}$.

Numerical discretization

Divide ∂D into N small boundary elements $\gamma_1, \gamma_2, \cdots, \gamma_N$, typically linear triangle or quadrilateral, so eqn. (4) is discretized, that

$$\frac{u(\bar{x}_i)}{2} + \sum_{j=1}^{N}\int_{\gamma_j} \frac{\partial G(\bar{y},\bar{x}_i)}{\partial n(\bar{y})}u_j dS(\bar{y})$$
$$= sk\sum_{j=1}^{N}\int_{\gamma_j} G(\bar{y},\bar{x}_i)\, v_n(\bar{x}_j) dS(\bar{y}), \ (\bar{x}_i \in \partial D) \tag{6}$$
$$u(\bar{x}_i) + \sum_{j=1}^{N}\int_{\gamma_j} \frac{\partial G(\bar{y},\bar{x}_i)}{\partial n(\bar{y})}u_j dS(\bar{y})$$
$$= sk\sum_{j=1}^{N}\int_{\gamma_j} G(\bar{y},\bar{x}_i)\, v_n(\bar{x}_j) dS(\bar{y}), \ (\bar{x}_i \in D) \tag{7}$$

eqn.(6) are a set of N linear equations to determine the N unknown variables $u_1, u_2, \cdots u_N$. To solve the acoustic field variables in eqn. (7), the boundary variables in eqn. (6) has to be first determined. Herein exterior acoustic problems in free space is considered and following expressions are defined:

$$\mathbf{u} \triangleq [u(\bar{x}_1), u(\bar{x}_2), \cdots, u(\bar{x}_N)]^T$$
$$\mathbf{v_n} \triangleq [v_n(\bar{x}_1), v_n(\bar{x}_2), \cdots, v_n(\bar{x}_N)]^T$$
$$[\mathbf{A}]_{ij} \triangleq \int_{\gamma_j} \frac{\partial G(\bar{y},\bar{x}_i)}{\partial n(\bar{y})}\, dS(\bar{y}) = a_{ij}$$
$$[\mathbf{B}]_{ij} \triangleq sk\int_{\gamma_j} G(\bar{y},\bar{x}_i) dS(\bar{y}) = b_{ij}$$

So the linear system of eqn. (6) is:

$$(\mathbf{I}/2 + \mathbf{A})\,\mathbf{u} = \mathbf{B}\,\mathbf{v_n} \tag{8}$$

where $\mathbf{I}$ denotes the diagonal matrix of order N.
The eqn. (8) of linear system shows that the Neumann problem is more stable than Dirichlet problem[10], this can be related to the shift in the singular value spectrum introduced by addition of the dialogue matrix $\mathbf{I}/2$ .However, when source point coincides with or closes to field point, singularity and hyper-singularity of Green function and its derivative is inevitable, so advanced method like self-adaptive Gauss quadrature is needed to deal with this singularity which will be discussed in next section.

Self-adaptive quadrature of quadratic quadrilateral boundary element

Visser [10] give a local mesh refinement scheme to solve the Helmholtz hyper-singular and singular integral. In fact, this local refinement scheme is however invalid for hyper-singular integral because the convergence behavior of this type of quadrature is poor. In this paper, a self-adaptive global mesh refinement scheme is introduced to solve singular integral $\int_{\gamma_j} G(\bar{y},\bar{y}_i) dS_j$, see Figure 1. For hyper-singular integral $\int_{\gamma_j} \partial G(\bar{y},\bar{y}_i)/\partial n(\bar{y}) dS_j$, as an analytic solution exists, so it won't be discussed in this paper. Herein considering quadratic quadrilateral(QUAD8) boundary element is adopted, by coordinate transformation, the integration on QUAD8 can be transformed to a standard square area by interpolation , as illustrated in Figure 1.

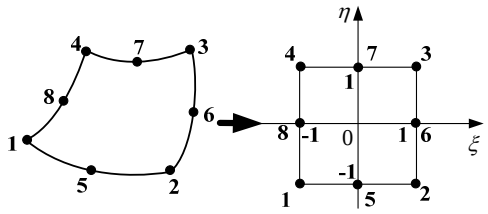

Figure 1. Coordinate transformation of a quadratic quadrilateral element to a standard square element

The shape function of each node is:

$$\begin{cases} N_j = (1+\xi_j\xi)(1+\eta_j\eta)/4 & j = 1,2,3,4 \\ N_j = (1-\xi^2)(1+\eta_j\eta)/2 & j = 5,7 \\ N_j = (1+\xi_j\xi)(1-\eta^2)/2 & j = 6,8 \end{cases} \tag{9}$$

So the variables and their derivatives on QUAD8 can be interpolated via shape function, that:

$$x = \sum_{j=1}^{8} N_j(\xi,\eta)\, x_j, y = \sum_{j=1}^{8} N_j(\xi,\eta)\, y_j$$
$$\partial x/\partial\xi = \sum_{j=1}^{8} N_{\xi j}(\xi,\eta)\, x_j, \partial x/\partial\eta = \sum_{j=1}^{8} N_{\eta j}(\xi,\eta)\, x_j$$
$$\partial y/\partial\xi = \sum_{j=1}^{8} N_{\xi j}(\xi,\eta)\, y_j, \partial y/\partial\eta = \sum_{j=1}^{8} N_{\eta j}(\xi,\eta)\, y_j$$

Where (x_j, y_j) is node coordinate, $N_{\xi j}$, $N_{\eta j}$ is the partial derivative of shape function on ξ,η , respectively. So:

$$I = \int_S f(x,y)\, dxdy = \int_{-1}^{1}\int_{-1}^{1} f[x(\xi,\eta), y(\xi,\eta)]\lambda(\xi,\eta)\, d\xi d\eta \tag{10}$$

With $$\lambda(\xi,\eta) = \frac{\partial x}{\partial\xi}\frac{\partial y}{\partial\eta} - \frac{\partial x}{\partial\eta}\frac{\partial y}{\partial\xi} \tag{11}$$

Now the attention is on how to accurately calculate eqn.(10) by Gauss quadrature. Herein, an adaptive mesh refinement scheme is introduced to solve this problem. Figure 2 illustrates the flowchart of the adaptive Gauss quadrature. In this technique, the initial boundary element (father element) is divided into four refined elements (children elements), each children element can further be refined again. In this way, the initial coarse boundary element is decomposed into refined small elements. In each stage of the mesh refinement, an approximate solution can be obtained. Generally multi-refinement of the boundary element is needed to get a convergent solution at a given allowable tolerance, then the integration solution is returned to the initial element and the temporary children elements in each level of refinement are

cleared simultaneously, so the adaptive quadrature scheme is also called mesh-less scheme. In the process of adaptive Gauss quadrature, only a small memory of computer is needed, and even coarse initial boundary elements can get accurate solution. Take the advantage of this technique, it provides an effective tool to deal with large scale problems. So, eqn.(10) can further be expressed as:

$$I = \sum_{i=1}^{Ng} \sum_{j=1}^{N_g} H_{ij} \lambda(\xi_i, \eta_j) f(\xi_i, \eta_j) \tag{12}$$

Where (ξ_i, η_j) are Gaussian point, H_{ij} is the corresponding weight, $N_g = 4^{Nr}$ is the number of Gaussian points, Nr is the number of element refinement level.

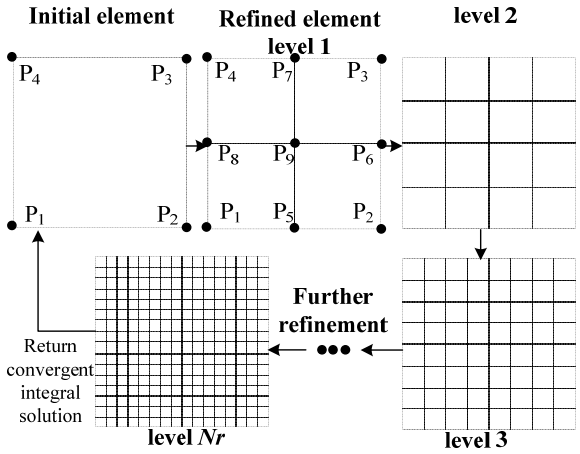

Figure 2. Flowchart of the self-adaptive Gauss quadrature on refined square element

Next, we will determine the Gaussian points and corresponding weight of children element at each level of refinement by a Multi-level boundary element refinement algorithm.

Multi-level boundary element refinement algorithm

In the first level of element refinement as shown in Figure 2, the initial *father element* $P_1P_2P_3P_4$ is divided into four *children elements* $P_1P_5P_9P_8$, $P_5P_2P_6P_9$, $P_9P_6P_3P_7$ and $P_8P_9P_7P_4$, five new nodes P_5,P_6 ,P_7,P_8,P_9 are born. The Gaussian points of each element are determined by element nodes, and each children element node can be calculated out via node transform matrices $\mathbf{T_1}, \mathbf{T_2}, \mathbf{T_3}, \mathbf{T_4}$, for example:

$$[\mathbf{x_1}, \mathbf{x_5}, \mathbf{x_8}, \mathbf{x_9}]^T = \mathbf{T_1 X_{n0}}, [\mathbf{x_5}, \mathbf{x_2}, \mathbf{x_6}, \mathbf{x_9}]^T = \mathbf{T_2 X_{n0}}$$
$$[\mathbf{x_9}, \mathbf{x_6}, \mathbf{x_3}, \mathbf{x_7}]^T = \mathbf{T_3 X_{n0}}, [\mathbf{x_8}, \mathbf{x_9}, \mathbf{x_7}, \mathbf{x_4}]^T = \mathbf{T_4 X_{n0}}$$

$$\mathbf{T_1} = \begin{bmatrix} 1 & 0 & 0 & 0 \\ 1/2 & 1/2 & 0 & 0 \\ 1/4 & 1/4 & 1/4 & 1/4 \\ 1/2 & 0 & 0 & 1/2 \end{bmatrix}, \mathbf{T_2} = \begin{bmatrix} 1/2 & 1/2 & 0 & 0 \\ 0 & 1 & 0 & 0 \\ 0 & 1/2 & 1/2 & 0 \\ 1/4 & 1/4 & 1/4 & 1/4 \end{bmatrix}$$

$$\mathbf{T_3} = \begin{bmatrix} 1/4 & 1/4 & 1/4 & 1/4 \\ 0 & 1/2 & 1/2 & 0 \\ 0 & 0 & 1 & 0 \\ 0 & 0 & 1/2 & 1/2 \end{bmatrix}, \mathbf{T_4} = \begin{bmatrix} 1/2 & 0 & 0 & 1/2 \\ 1/4 & 1/4 & 1/4 & 1/4 \\ 0 & 0 & 1/2 & 1/2 \\ 0 & 0 & 0 & 1 \end{bmatrix}$$

Where $\mathbf{X_{n0}} = [\mathbf{x_1}, \mathbf{x_2}, \mathbf{x_3}, \mathbf{x_4}]^T$ is initial nodes coordinate matrix, $\mathbf{X_i}$ is node coordinate vector.

Once the children elements node are known, the Gaussian point can be determined via Gaussian point transform matrices, herein one Gaussian point of each element is chosen, for example:

$$\mathbf{x_{g_0}} = \mathbf{Q_0 X_{n0}} \ , \ \mathbf{x_{g_1}} = \mathbf{Q_1 X_{n0}}$$

$$\mathbf{Q_0} = [1/4, 1/4, 1/4, 1/4], \mathbf{Q_1} = \begin{bmatrix} 3/4 & 0 & 1/4 & 0 \\ 0 & 3/4 & 0 & 1/4 \\ 1/4 & 0 & 3/4 & 0 \\ 0 & 1/4 & 0 & 3/4 \end{bmatrix}$$

Where $\mathbf{x_{g_0}}$ is initial element Gaussian point, $\mathbf{x_{g_1}}$ are first level refined element Gaussian points. In order to determine the N^{th}-level children elements Gaussian point by MATLAB codes, herein four algorithm operators are defined as following:

" $\otimes$ " : represents a matrix left-multiply a cell matrix;
" $\oplus$ " : represents a matrix right-multiply a cell matrix;
" @ " : represents a cell matrix multiply a cell matrix;
" $\wedge$ " : represents exponential multiply of a cell matrix.

For example:

$$\mathbf{A} \otimes [\mathbf{B_1}, \mathbf{B_2}, \mathbf{B_3}, \mathbf{B_4}] = [\mathbf{AB_1}, \mathbf{AB_2}, \mathbf{AB_3}, \mathbf{AB_4}]$$
$$[\mathbf{B_1}, \mathbf{B_2}, \mathbf{B_3}, \mathbf{B_4}] \oplus \mathbf{A} = [\mathbf{B_1 A}, \mathbf{B_2 A}, \mathbf{B_3 A}, \mathbf{B_4 A}]$$
$$[\mathbf{A_1}, \mathbf{A_2}] @ [\mathbf{B_1}, \mathbf{B_2}] = [\mathbf{A_1 B_1}, \mathbf{A_2 B_1}, \mathbf{A_1 B_2}, \mathbf{A_2 B_2}]$$
$$[\mathbf{A_1}, \mathbf{A_2}, \mathbf{A_3}]^{\wedge 2} = [\mathbf{A_1}, \mathbf{A_2}, \mathbf{A_3}] @ [\mathbf{A_1}, \mathbf{A_2}, \mathbf{A_3}]$$

So, with the above algorithm operator, the node coordinate and element Gaussian point of each level can be expressed as:

$$\mathbf{X_{n1}} = \mathbf{Tr} \oplus \mathbf{X_{n0}} \ , \ \mathbf{X_{g1}} = \mathbf{Q_1} \otimes \mathbf{X_{n0}}$$
$$\mathbf{X_{n2}} = \mathbf{Tr} @ \mathbf{X_{n1}} = \mathbf{Tr}^{\wedge 2} \oplus \mathbf{X_{n0}} \ , \mathbf{X_{g2}} = \mathbf{Q_1} \otimes \mathbf{X_{n1}} = \mathbf{Q_1} \otimes \mathbf{Tr} \oplus \mathbf{X_{n0}}$$
$$\mathbf{X_{n3}} = \mathbf{Tr}^{\wedge 3} \oplus \mathbf{X_{n0}} \ , \mathbf{X_{g3}} = \mathbf{Q_1} \otimes \mathbf{Tr}^{\wedge 2} \oplus \mathbf{X_{n0}}$$
$$\vdots$$
$$\mathbf{X_{nN}} = \mathbf{Tr}^{\wedge N} \oplus \mathbf{X_{n0}} \ , \ \mathbf{X_{gN}} = \mathbf{Q_1} \otimes \mathbf{Tr}^{\wedge (N-1)} \oplus \mathbf{X_{n0}} \tag{13}$$

Where $\mathbf{Tr} = [\mathbf{T_1}, \mathbf{T_2}, \mathbf{T_3}, \mathbf{T_4}]^T$ is the node transform cell matrix, $\mathbf{X_{ni}}, \mathbf{X_{gi}}$ is the i^{th}-level *children element* nodes and Gaussian point coordinate matrix, respectively.
The weight of the N^{th} level children elements Gaussian point is $w_N = S_f / 4^N$, and S_f is the initial square element area. In this way, once $\mathbf{X_{n0}}$ is given, $\mathbf{X_{gN}}$ can be determined and integration of eqn.(12) can easily be calculated out.

Convergence behavior of the adaptive quadrature validation

(1) Singular integral kernel function: *f=1/r*.

Let I_i denote the i^{th} level refined Gauss quadrature, I_{i1} denotes the quadrature on the area that close to singular point, as shown in Figure 4, I_{i2} denotes the quadrature on non-singular area, and $I_i = I_{i1} + I_{i2}$, the length of the first stage square is a, area $S = 4a^2$, so:

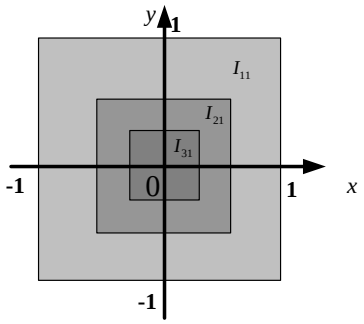

Figure 3. Integration on refined singular element.

$$I_1 = I_{11} + I_{12} = I_{11} + 0 = \sum_{i=1}^{4} \frac{w_1}{r(x_{1i}, y_{1i})} = 4\sqrt{2}a$$

$$I_2 = I_{21} + I_{22} < (S - \frac{S}{4})\frac{1}{a/2} + I_{22} = 6a + \sum_{i=1}^{4} \frac{w_2}{r(x_{2i}, y_{2i})} = (6 + 2\sqrt{2})a$$

$$I_2 = I_{21} + I_{22} > (S - \frac{S}{4})\frac{1}{a} + I_{22} = 3a + \sum_{i=1}^{4} \frac{w_2}{r(x_{2i}, y_{2i})} = (3 + 2\sqrt{2})a$$

$$I_N = I_{21} + (I_{31} - I_{21}) + (I_{41} - I_{31}) + \cdots + (I_{N1} - I_{N-1,1}) + I_{N2}$$

$$< 6a + 3a + 3a/2 + \cdots 6a/2^{N-2} + I_{N2} = 12(1 - \frac{12 - 4\sqrt{2}}{2^{N-1}})a$$

$$I_N = I_{21} + (I_{31} - I_{21}) + (I_{41} - I_{31}) + \cdots + (I_{N1} - I_{N-1,1}) + I_{N2}$$

$$> 3a + 3a/2 + \cdots 3a/2^{N-2} + I_{N2} = 6(1 - \frac{6 - 4\sqrt{2}}{2^{N-1}})a$$

So as N goes to infinite, the refined Gauss quadrature will convergent at a constant value, see Figure 4(a).

(2) Hyper-singular integral kernel function: $f=1/r^2$.

When adaptive Gauss quadrature is applied to Helmholtz hyper-singular integral as Visser [10] did, it is found that this adaptive quadrature is invalid in that:

$$I_N = I_{21} + (I_{31} - I_{21}) + \cdots + (I_{N1} - I_{N-1,1}) + I_{N2}$$

$$< 12 + 12 + \cdots 12 + I_{32} = 12(N-1) + \sum_{i=1}^{4} \frac{w_N}{r^2(x_{Ni}, y_{Ni})} = 12(N-1) + \frac{4\sqrt{2}}{2^{N-1}}a$$

$$I_N = I_{21} + (I_{31} - I_{21}) + \cdots + (I_{N1} - I_{N-1,1}) + I_{N2}$$

$$> 3 + \cdots 3 + I_{N2} = 3(N-1) + \sum_{i=1}^{4} \frac{w_N}{r^2(x_{Ni}, y_{Ni})} = 3(N-1) + \frac{4\sqrt{2}}{2^{N-1}}a$$

So as N goes to infinite, the refined Gauss quadrature on hyper-singular integral will not convergent at a finite value, see Figure 4(b). In this way, Visser's adaptive scheme is inapplicable to hyper-singular integration. In fact a analytical solution of the Helmholtz hyper-singular integration can be obtained by singularity-decomposition scheme which won't be discussed here in detail.

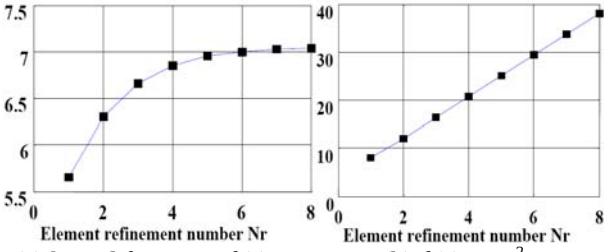

(a) kernel function: $f(r) = 1/r$ (b) $f(r) = 1/r^2$

Figure 4. Adaptive quadrature convergence behaviour of different kernel function.

NUMERICAL VALIDATION

In this section, the performance of the self-adaptive quadrature is investigated. A lot of publications and papers on boundary element method for acoustic radiation choose the pulsating sphere as a validation tool since the simple analytic solution is available in this case. Herein the radius of the sphere is 0.1m with uniformly pulsating velocity 0.001m/s, and the propagation medium is water with sound speed 1500m/s, density 1000kg/m^3. Firstly the BEM model of the sphere source is made, and then self-adaptive quadrature is used to calculate singular integral. On each refinement level an approximate integral solution is obtained and compared to the integration solution of previous level. The convergence behaviour of the integral solution in each refinement level is defined by *ERRO:*

$$ERRO = \left|(I_{i+1} - I_i)/I_i\right|, (i = 1, 2, \cdots, N_{\max} - 1) \quad (14)$$

When the relative error *ERRO* convergent at a given allowable error i.e. $ERRO_{\max}$,usually 1e-4 which is sufficient satisfactory for the engineering application, no further refinement is necessary. By the way, the maximum refinement number $N_{\max}$ is prescribed to prevent excessive number of temporary elements. It is commended that $N_{\max}$ should be between 4 and 8 [10] By far the code of self-adaptive BEM methodology has been worked out and successfully used to predict underwater radiated noise. Figure 5 illustrates the convergence behaviour and CPU(Duo CPU,@2.33GHz,8GB memory) run time of the self-adaptive BEM quadrature with the refinement level. So to ensure both accuracy and time-cost, optimum refinement number can be determined at $N_{\max} = 6$. Figure 6 illustrate the numerical solution and analytic solution of the radiated sound pressure level at near-field and far-field from 10Hz to 1KHz. Figure 7 demonstrates sound directivity at several frequencies, the results show that numerical solutions agree well analytic solution with maximum error less than 1.5dB.

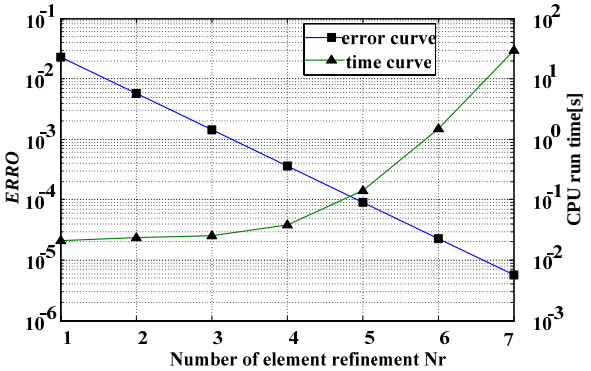

Figure 5. Convergence behaviour and CPU run time of the self-adaptive BEM quadrature.

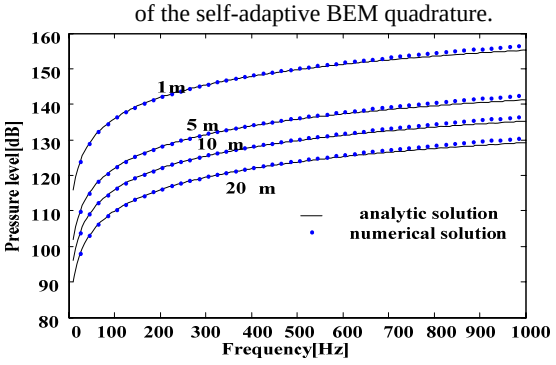

Figure 6. Sound radiation pattern of the source

at different distance.

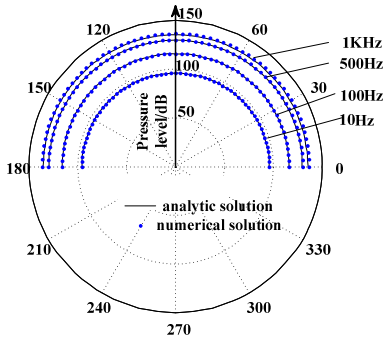

Figure 7. Sound directivity at 10m from sphere center at 0 to 180^o.

APPLICATION TO PREDICT SUBMARINE UNDERWATER VIBRATION NOISE

In this section , the BEM based on adaptive scheme and FEM are combined to predict submarine underwater vibration noise. FEM is used to calculate the vibration response of the submarine hull, BEM is used to predict the hull vibration induced underwater noise.

FE and BE model

To achieve a reliable prediction of engine induced underwater noise, a detailed 1:1 full submarine model is required to be taken into account. In addition, considering underwater radiated noise due to the excitation of engine source to the hull, the level of radiated sound power depends on the interaction of structure and water, so the fluid-structure interaction must be also taken into account to simulate the effects of the structure surrounding fluid. Due to the fact that our major concern here is the engine unbalanced force induced hull vibration and underwater noise, only the engine vibration source is considered. Figure 8 depicts the major physical dimensions of the submarine, The hull is stiffened by 4 bulkheads, the engine weighted 230kg, and is attached to two sets of periodic-isolators mounted at the stern part of the structure. The excitation force is acted on periodic-isolators axysimmetrically, and the vibration is transmitted to the hull via periodic-isolator and finally radiate underwater noise. Herein all periodic-isolators are modeled as 3-DOF, i.e. three translational springs with properly defined damping coefficients, and the stiffness of the periodic-isolator is Kx=5E+8N/m, Ky=Kz=1e+9N/m, the damping ratio is 0.09, the excited force is 100N. The main physical parameters of the structure are listed in Table 1.

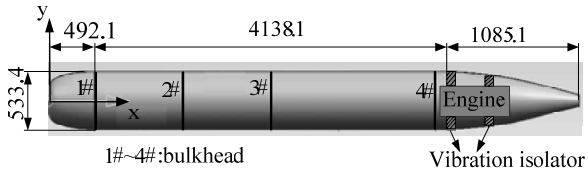

Figure 8. Geometry of the submarine (unit: mm)

Table 1. Main parameters of the structure

	Thickness (m)	Young's modulus (Mpa)	Poisson's ratio	Density (kg m-3)
Hull	7E-3	2.1E+5	0.33	7850
Bulkhead	6E-3	2.1E+5	0.31	7850

FEM as a good tool for study of structure vibration has been widely used in underwater vehicle vibration-noise prediction [11,12], while M. Caresta [13,14] investigated the structural and acoustic responses of a submarine hull under axial excitation by analytical method. Herein, ANSYS is used to research the underwater structure vibration numerically. Figure 9(a) illustrates the FE model of the structure and surrounding coupling fluid. The sphere radius of the fluid domain is ten times of the structure length, the fluid element size that contact with the structure is about 29mm, and the maximum size of the un-contact element is less than 625mm. In addition, in order to capture the vibration details, the closure shell elements of the submarine are refined as depicts in Figure 9 (b) and (c). The total number of the structure elements is 24121.

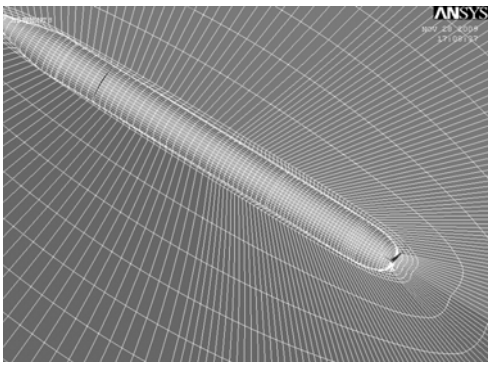

(a)

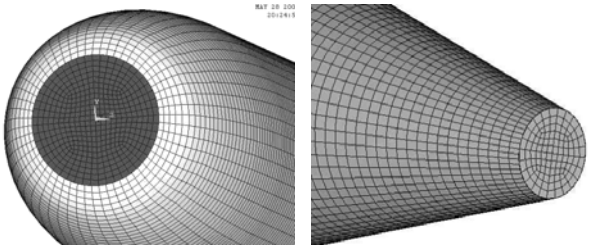

(b) (c)

Figure 9. FEM model of the structure and surround- ing coupling fluid. (a)structure-fluid interaction Finite element; (b) local refined element of the fore;(c)local refined element of the stern.

The BE model is abstracted from the FE model of structure hull which consists of 7602 boundary elements, and the structure boundary vibration velocities calculated from FEM are used as the boundary condition of the boundary element model, so BEM can be used to predict underwater radiated noise.

Numerical results and discussion

Figure 10 shows the predicted results of submarine hull boundary and near-field sound pressure distribution at the plane (2m*6m in size) that 1m above the center plane of the structure. It is showed that the sound pressure behaves much stronger at the excitation location than other locations at different frequencies. In addition, from the sound radiation color map, the high sound pressure area can be easily detected as the arrows direct in Figure 10. So in this way, the location of vibration source can be roughly determined when near-field sound pressure is calculated and visualized, and this area relates to source identification which won't be discussed here.

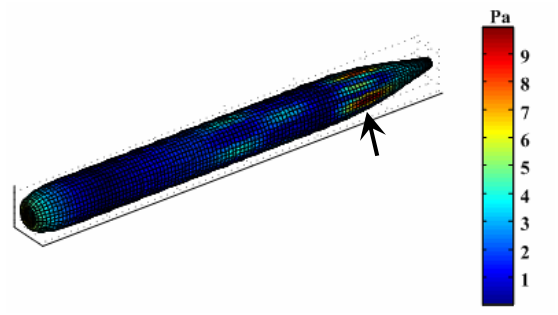

(a)

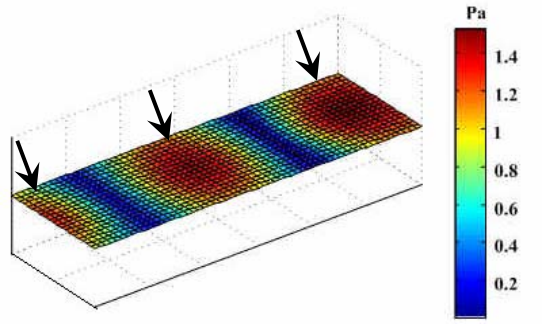

(b)

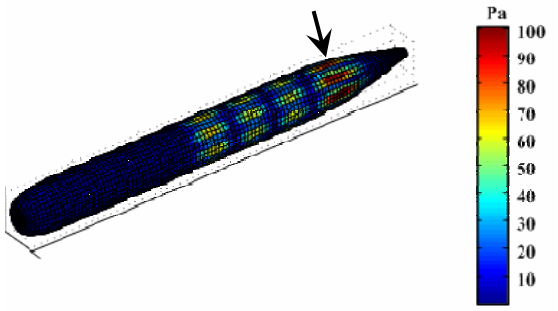

(c)

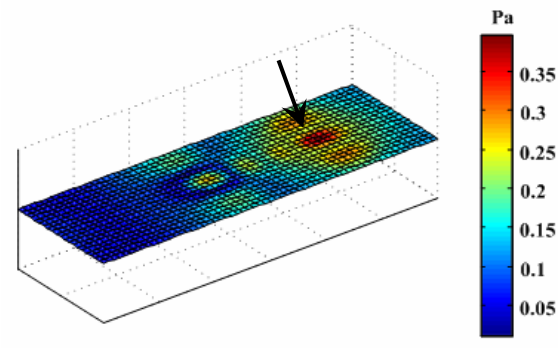

(d)

Figure 10. Structure boundary and near-field (at 1m) sound pressure distribution color map.(a) boundary color map at 268Hz,(b)near-field color map at 268 Hz,(c)boundary color map at 312Hz,(d)near-field color map at 312Hz.

By analyzing the color map in Figure 10, the high sound pressure area can be easily localized, but it cannot provide detailed information about the radiated sound power transmitted from the vibrated engine to structure hull. So in order to quantificationally evaluate the submarine underwater radiated noise, both the sound pressure and sound velocity on each boundary element of the submarine hull should be considered. In this way the radiated sound power level is defined as follows:

$$P_R = \frac{1}{2}\Re[\sum_{j=1}^{N_{elem}} \int_{\gamma_j} u(\bar{x}_j) v_n^*(\bar{x}_j)\, dS] \tag{15}$$

$$LP_R = 10\log_{10} P_R / P_{R\_ref}\ (dB) \tag{16}$$

where $\Re(\bullet)$ denotes real part of the summation, * denotes conjugate complex, P_R is the radiated sound power, LP_R is the sound power level, $P_{R\_ref} = 1\times10^{-18} W$ is the reference radiated sound power in water.

Figure 11 depicts the radiated sound power level of the submarine hull from 0Hz to 400Hz for different isolator stiffness. For the solid line, the spectrum peaks are found at 128Hz, 214Hz, 248Hz,268Hz,312Hz and 328Hz, and the maximum radiated sound power level is about 100dB at 312Hz and 328Hz. In order to control the noise level at 312Hz and 328Hz without changing the property of the structure, we can further consider the impact of the rubber isolator stiffness to underwater radiated sound power with the same excitation of the engine. Herein altering the rubber isolator's stiffness $K = \{K_x, K_y, K_z\}$ into $K/2$, the sound radiation pattern of the submarine changes simultaneously, see the dashed line in Figure 11. Results show that, reduction of the rubber isolator stiffness does great benefit to the reduction of radiated sound power level at 66.7Hz to 400Hz, this can be seen from Figure 11 that when the stiffness changes, the maximum radiated sound power level is about 90dB at 268Hz and 328Hz, so nearly 10dB is reduced at 328Hz, 13dB at 312Hz, however,10dB increased at 268Hz, and the sound power level increases 10dB on average at 0Hz to 66.7Hz. So, when stiffness of the periodic-isolator changes, the characteristic of the sound power spectrum changes too, and reduction of the engine periodic-isolator's stiffness can effectively transfer the sound power of peak frequencies to band-spectrum and the vibration noise of the line spectrum is controlled.

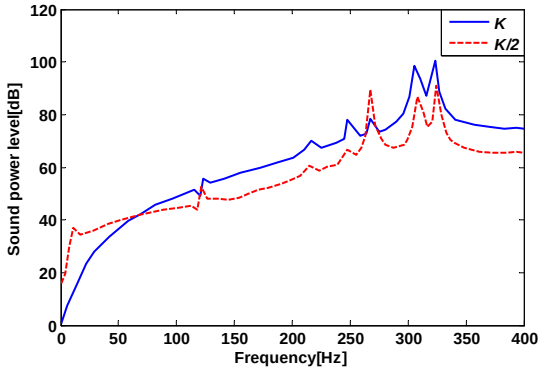

Figure 11. Radiated sound power level of the structure for different rubber isolator stiffness.

CONCLUSION

Self-adaptive BEM quadrature can well improve the singularity of HIE and reduce the computation effort. The refined temporary children elements just played a "springboard" role in the singular integral calculation, it did no contribution to the total number of boundary elements. When the adaptive quadrature scheme is applied to singular integration, the solution convergence behaves well, and when applied to hyper-singular integration, the solution convergence is poor. So, in order to accurately predict near-

field sound pressure, the adaptive scheme should be carefully used. Then BEM coupled with FEM were applied to predict underwater vehicle vibration-noise considering fluid-structure interaction effects. By visualization the near-field sound pressure distribution, high sound pressure area was localized. Finally, the underwater radiated sound power was calculated and the peak frequencies were identified. Reduction of the engine periodic-isolator's stiffness can effectively transfer the sound power of peak frequencies to band-spectrum and the vibration noise of the line spectrum is controlled.

REFERENCES

1 Jaswon M.A, Symm G.T, Integral Equation Methods in Potential Theory and Elastostastics Academic Press, New York, 1977.

2 Cruse T.A, "A Direct formulation and Numerical solution of the General Transient elastodynamic Problem". J.Math. Anal. and Appl 22,.341-355 (1968).

3 Chen L.H and Schweikert D.G, "Sound Radiation from An Arbitrary Body". J. Acous. Soc. Am. 35, 1626-1632 (1963).

4 Chertock G, "Sound Radiation from Vibration Surface". J. Acous. Soc. Am. 36, 1305-1313 (1964).

5 Schenck H.A, "Improved integral formulation for acoustic radiation problems". J.Acous. Soc. Am. 44, 41–58 (1968).

6 Burton A.J and Miller G.F, "The application of integral equation methods to the numerical solution of some exterior boundary–value problems", Proceedings of the Royal Society of London 323, 201–220 (1971).

7 S. Marburg and T. W. Wu, "Chapter 15: Treating the Phe nomenon of Irregular Frequency" in *Computational Acoustics of Noise Propagation in Fluids-Finite and Boundary Element methods*, ed. Steffen Marburg and Bodo Nolte (Heidelberg Publication, Berlin, 2008) pp. 411-432.

8 P. Kolm and V.Rokhlin, "Numerical Quadratures for Sin gular and Hyper-singular Integrals". Computers and Mathematics with Applications 41, 327-352 (2001).

9 M. Carley. "Numerical quadrature for singular and hyper-singular integrals in boundary element methods". SIAM Journal on Scientific Computing 29(3), 1207–1216 (2007).

10 Visser R, "A Boundary Element Approach to Acoustic Radiation and Source Identification". PhD thesis, University of Twente (2004).

11 H. Zheng and G. R. Liu, "FEM/BEM analysis of diesel piston-induced ship hull vibration and underwater noise". Applied Acoustics 62, 341-358 (2001).

12 Z. Tong and Y. Zhang. "Dynamic behavior and sound transmission of a fluid-structure coupled system using the direct-BEM/FEM". Journal of Sound and Vibration 299, 645-655 (2007).

13 M. Caresta, "Structural and acoustic response of a sub-merged vessel", PhD thesis, University of New South Wales (2009).

14 M. Caresta and N.J. Kessissoglou, "Acoustic signature of a submarine hull under harmonic excitation", Applied Acoustics 71, 17-31 (2010).